Redox Biology 76 (2024) 103351

Contents lists available at ScienceDirect

Redox Biology

journal homepage: www.elsevier.com/locate/redox

PPARγ drives mitochondrial stress signaling and the loss of atrial cardiomyocytes in newborn mice exposed to hyperoxia

E. David Cohen [a,**], Kyle Roethlin [a], Min Yee [a], Collynn F. Woeller [b], Paul S. Brookes [c], George A. Porter Jr. [a], Michael A. O'Reilly [a,*]

[a] Department of Pediatrics, School of Medicine and Dentistry, The University of Rochester, Rochester, NY 14642, USA
[b] Department of Ophthalmology, School of Medicine and Dentistry, The University of Rochester, Rochester, NY 14642, USA
[c] Department of Anesthesiology, School of Medicine and Dentistry, The University of Rochester, Rochester, NY 14642, USA

ARTICLE INFO

Keywords:
Cardiomyocytes
Hyperoxia
Peroxisome proliferator activated receptor
Mitochondria
Reactive oxygen species

ABSTRACT

Diastolic dysfunction is increasingly common in preterm infants exposed to supplemental oxygen (hyperoxia). Previous studies in neonatal mice showed hyperoxia suppresses fatty acid synthesis genes required for proliferation and survival of atrial cardiomyocytes. The loss of atrial cardiomyocytes creates a hypoplastic left atrium that inappropriately fills the left ventricle during diastole. Here, we show that hyperoxia stimulates adenosine monophosphate-activated kinase (AMPK) and peroxisome proliferator activated receptor-gamma (PPARγ) signaling in atrial cardiomyocytes. While both pathways can regulate lipid homeostasis, PPARγ was the primary pathway by which hyperoxia inhibits fatty acid gene expression and inhibits proliferation of mouse atrial HL-1 cells. It also enhanced the toxicity of hyperoxia by increasing expression of activating transcription factor (ATF) 5 and other mitochondrial stress response genes. Silencing PPARγ signaling restored proliferation and survival of HL-1 cells as well as atrial cardiomyocytes in neonatal mice exposed to hyperoxia. Our findings reveal PPARγ enhances the toxicity of hyperoxia on atrial cardiomyocytes, thus suggesting inhibitors of PPARγ signaling may prevent diastolic dysfunction in preterm infants.

1. Introduction

Approximately 10 % of births occur before 37 weeks of gestation and are thus considered preterm. People born preterm are at risk of developing pulmonary hypertension and heart failure as young adults [1–3]. An analysis of Swedish National Patient Registry data found that young adults who were born prior to 28 weeks of gestation had 17x higher rates of heart failure than those born full term [3]. Two studies looking at mortality of 4–6 million citizens in 4 Nordic nations found a 2-fold increase in cardiovascular related mortality among adults born preterm and a nearly 5-fold increase in adults born extremely preterm [4,5]. MRI and echocardiographic imaging showed adults born preterm have altered ventricular morphology, left sided diastolic dysfunction and lower cardiac output than controls due to reduced left ventricular end-diastolic volume [6,7]. The risk of early heart failure is highest in severely preterm infants who often need supplemental oxygen (hyperoxia) to survive, and the duration of oxygen treatment has been correlated with the severity of heart disease [8,9].

Exposing newborn rodents to hyperoxia can permanently affect cardiac function later in life. Systolic and diastolic dysfunction are seen in neonatal rats exposed to hyperoxia between birth and postnatal day (PND) 14 [10,11]. While these changes resolved by PND 35, rats previously exposed to hyperoxia developed right ventricular (RV) hypertrophy with reduced RV ejection fraction by 1 year of life [12]. These long-term deficits in cardiac function have been attributed to the effects of hyperoxia on mitochondrial function [11,12]. The transition to breathing oxygen at birth increases the production of mitochondrial reactive oxygen species (mitoROS), which can inhibit ventricular cardiomyocyte proliferation by oxidizing DNA and causing them to undergo terminal maturation [13]. Neonatal hyperoxia may thus initiate heart failure by causing cardiomyocytes to stop proliferating and undergo terminal maturation before enough cells are produced to maintain normal adult cardiac function. Consistent with this idea, a postmortem analysis of preterm infants found that cardiomyocyte proliferation was significantly lower in their hearts compared to term infants, while cardiomyocyte size and matrix composition were unaffected [14]. Hyperoxia also causes systemic and pulmonary hypertension in rats and mice

* Corresponding author. Department of Pediatrics, Box 850, USA.
** Corresponding author. Department of Pediatrics, Box 631, USA.
E-mail addresses: ethan_cohen@urmc.rochester.edu (E.D. Cohen), michael_oreilly@urmc.rochester.edu (M.A. O'Reilly).

https://doi.org/10.1016/j.redox.2024.103351
Received 7 June 2024; Received in revised form 22 August 2024; Accepted 9 September 2024
Available online 12 September 2024

Abbreviations

AICAR	5-Aminoimidazole-4-carboxamide ribonucleoside
AMP	Adenosine monophosphate
AMPK	Adenosine monophosphate-activated kinase
ANOVA	Analysis of variance
ATF	Activating transcription factor
ATM	Ataxia telangiectasia mutated
ATP	Adenosine triphosphate
Cl-Casp3	Cleaved caspase 3
DAPI	4′,6-diamidino-2-phenylindole
Ddit3	DNA damage inducible transcript 3
DMSO	Dimethyl sulfoxide
DNA	Deoxyribonucleic acid
Edu	5-Ethynyl-2′-deoxyuridine
ERK	Extracellular signal-regulated kinase
ER	Endoplasmic reticulum
Fasn	Fatty acid synthase
Fabp4	Fatty acid binding protein 4
4-HHE	4-Hydroxyhexenal
4-HNE	4-Hydroxynoneanal
HRP	Horse radish peroxidase
Hspa	Heat shock protein
KEGG	Kyoto Encyclopedia of Genes and Genomes
mRNA	Messenger ribonucleic acid
MAPK	Mitogen-activated protein kinase
MRI	Magnetic resonance imaging
mitoROS	Mitochondrial reactive oxygen species
MitoUPR	Mitochondrial unfolded protein response
NT	Non-targeting
PI	Propidium iodide
PND	Postnatal day
PPARγ	Peroxisome Proliferator Activated Receptor-gamma
PPRE-Luc	Peroxisome proliferator response element-Luciferase
Prkaa2	Protein kinase AMP-activated catalytic subunit alpha 2
qRT-PCR	Quantitative reverse transcriptase polymerase chain reaction
Scd1	Stearoyl-CoA desaturase 1
SD	Standard deviation
SREBP	Serum response element binding protein
Trib3	Tribble pseudo kinase 3
TNNI3	Troponin I3

that may contribute to cardiac disease [12,15,16]. Pulmonary capillary rarefaction seen in one year old mice exposed to hyperoxia as neonates may also contribute to ventricle hypertrophy, heart failure and early mortality [17]. Neonatal hyperoxia may thus cause heart failure through direct damage of proliferating cardiomyocytes and indirectly when it drives pulmonary and systemic hypertension that increases afterload on the injured heart.

Although focus has been on understanding how ventricular cardiomyocytes respond to hyperoxia, we have been investigating how it impacts atrial cardiomyocytes because diastolic dysfunction and reduced left ventricular end-diastolic volume is seen preterm infants prior to loss of cardiac output [18,19]. By exposing newborn mice to hyperoxia between PND0-4 and recovering in room air, we found that hyperoxia produces mitoROS that inhibits proliferation and survival of cardiomyocytes lining the pulmonary vein and extending into the left atrium. Loss of these cells creates a hypoplastic left atria that does not properly fill the left ventricle in diastole [20,21]. A transcriptomics analysis of left atria collected from newborn mice revealed hyperoxia suppresses expression of genes in the *de novo* fatty acid synthesis pathway, including fatty acid synthase (*Fasn*) and stearoyl-CoA desaturase 1 (*Scd1*) [20]. The same changes in fatty acid gene expression and proliferation were seen when neonatal human atrial explants or mouse atrial cardiomyocyte HL-1 cells were exposed to hyperoxia. Thus, hyperoxia directly causes diastolic dysfunction when it inhibits the proper expansion of left atrial cardiomyocytes. However, our understanding of how neonatal hyperoxia impairs cardiomyocyte expansion via changes in mitoROS and fatty acid synthesis is still incomplete.

To address this gap in knowledge, pathway analyses of our published Affymetrix datasets of mouse left atrial tissues was used to identify potential mechanisms by which neonatal hyperoxia suppresses fatty acid synthesis genes and impairs the postnatal expansion of atrial cardiomyocytes. Top candidates included the adenosine monophosphate activated protein kinase (AMPK) and peroxisome proliferation activator receptor (PPAR) signaling pathways, which were chosen for further study due to their critical roles in maintaining lipid homeostasis [22,23]. AMPK is activated by high AMP: ATP ratios in cells with low ATP. It restores energy balance by promoting β-oxidation and other catabolic processes and inhibiting anabolic processes like lipid synthesis. PPAR family nuclear receptors regulate genes involved in β-oxidation and fatty acid synthesis to balance lipid metabolism. The studies described herein therefore test how AMPK and PPAR signaling contributes to the effects of hyperoxia on the expression of fatty acid synthesis genes, proliferation, and survival of atrial cardiomyocytes in neonatal mice and in cultured mouse atrial HL-1 cardiomyocyte cells.

2. Materials and methods

2.1. Exposing mice to hyperoxia

C57BL/6J mice purchased from the Jackson Laboratories were used to generate pups that were exposed to room air (21 % oxygen) or hyperoxia (100 % oxygen) from birth to postnatal day (PND) 4 [24]. Lactating females were rotated between room air and hyperoxia daily to ensure their lungs were not injured by hyperoxia. Some mice were injected on with 5 μg/mg of the PPARγ antagonist GW9662 (Cayman Chemical Company, 70785) or vehicle (corn oil) on PND0 and PND2 [25]. On PND4, hearts of mice were removed and either fixed in 4 % paraformaldehyde, embedded in paraffin, and sectioned or used to isolate RNA and protein. All mice were housed in pathogen-free microisolator cages according to a protocol approved by the University Committee on Animal Resources (protocol number 2007-121E).

2.2. Exposing HL-1 cells to hyperoxia

HL-1 mouse atrial cardiomyocytes (Sigma-Aldrich, SCC065) were cultured in Claycomb media (Sigma-Aldrich, 51800C) as described [20]. This atrial cardiomyocyte cell line was derived from a subcutaneous cardiac tumor from transgenic mice expressing the simian virus 4 (SV40) large T antign targeted to atrial cardiomyocytes using the atrial natriuretic (ANF) promoter [26]. For siRNA silencing, HL-1 cells were transfected with 30 pM of pooled siRNA targeting *Prkaa2* or *Pparg* (Horizon Discovery, M-040809-01-0005 and M-040712-01-0005) using Lipofectamine RNAiMax (Thermo Fisher Scientific, 13778075). To assess PPARγ activity, cells were transfected with 1 μg of the PPARγ responsive firefly luciferase reporter PPRE-Luc (Addgene, 1015), 0.5 μg of constitutive *Renilla* luciferase reporter (Addgene, 118016) and 2 μg of either PPARγ1 expression vector (Addgene, 8886) or empty expression vector with Lipofectamine 2000 (Thermo Fisher Scientific, 11668027). After 24 h, 10 μ M rosiglitazone (Cayman Chemical Company, 71740) or vehicle (DMSO) was added to the media and cells placed in sealed plexiglass boxes flooded with room air (21 % O2, 5 % CO_2) or hyperoxia (95 % O2, 5 % CO_2) at a flow rate of 5 L/min. Additional cells were

treated with 0.5–2.0 mM of the AMPK activator 5-Aminoimidazole-4--carboxamide ribonucleoside (AICAR) in water and either 50 nM GW9662 in DMSO or DMSO alone as a vehicle control.

The expansion of cells in room air and hyperoxia was evaluated by plating cells in 96 well culture plates (ThermoFisher Scientific) at equal density and allowing them to attach overnight. One plate was then fixed prior to exposure (0 h) before the remaining were divided into two groups and exposed to room air or hyperoxia for 48 h with plates fixed every 12 h. Cells were stained with 4′,6-diamidino-2-phenylindole (DAPI) to nuclei and counted using a Celigo imaging cytometer (Nexcelom, 200-BFFL-5C). To examine proliferation, cells were labeled with 10 mM EdU 5-Ethynyl-2′-deoxyuridine (EdU) for 30 min before being fixed and stained using the Click-IT EdU Cell Proliferation Kit (ThermoFisher Scientific, C10637). Cells were then fixed and stained with Hoechst 33342 to label nuclei and imaged with an imaging cytometer to determine the percentage of EdU labeled cells. Dead cells were identified by adding 1 μg/ml of the DNA dye propidium iodide (PI) and 10 μg/ml Hoechst 33342 to the culture media. While Hoechst 33342 is membrane permeable and stains all cells, PI is membrane impermeable and only labels dead cells with disrupted membranes. After 30 min, cells were washed and imaged with an imaging cytometer to determine the percentage of dead cells in each well.

2.3. Assessing mitochondrial respiration

HL-1 cells transfected with either non-targeting (NT) or *Pparg* siRNA were exposed to room air or hyperoxia for 48 h. Since the release of oxygen absorbed by plastic in hyperoxia interferes with measurements of oxygen consumption, cells were replated at 2500 cells/well in 96-well assay plates containing unbuffered basal DMEM with 2.5 mM glucose, 1 mM pyruvate, 1 mM glutamine, and 1 mM carnitine. The oxygen consumption rate (OCR) of the cells in each well was measured with an Agilent Seahorse™ xFe96 Bioanalyzer, before and after the sequential addition of 1 μM oligomycin A, 0.25 μM FCCP, and 0.5 μM rotenone with 0.5 μM actinomycin A. Upon completion of the assay, cells were stained with Hoechst to label nuclei and counted with an imaging cytometer to normalize OCR readings to the numbers of cells in each well. OCR after the addition of rotenone and actinomycin A represents non-mitochondrial OCR. Basal OCR was calculated by subtracting the non-mitochondrial OCR from the OCR of cells in plain medium. ATP-linked OCR was calculated by subtracting the OCR of cells after the addition of oligomycin A from the OCR in plain medium. Protein leak was calculated by subtracting non-mitochondrial OCR from that of cells in oligomycin A containing medium. Maximum OCR was calculated by subtracting non-mitochondrial OCR from the OCR in FCCP containing medium. OCR values are reported in pmol/min/1000 cells. The numbers of wells examined for each condition were: NT siRNA in room air (N = 9) and hyperoxia (N = 7); Pparg siRNA in room air (N = 10) and hyperoxia (N = 8). Results are representative of three independent experiments with similar results.

2.4. Quantitative RT-PCR

RNA was reverse transcribed with the Maxima First Strand Synthesis Kit for RT-qPCR (ThermoFisher Scientific, K1641). Quantitative PCR (qPCR) was performed with iTaq Universal Syber Green Master Mix (Bio-Rad, 1725121) and the primers listed in Table 1. RNA from 3 independently transfected wells were examined for each primer and fold changes calculated using the ΔΔCT method with primers for the house keeping genes *Tbp* and *Polr2a* as endogenous controls. Fold changes were normalized to expression levels in room air exposed control cells.

2.5. Western blotting

The left atria of individual mice and HL-1 cells were lysed in 2X Laemmli buffer (Bio-Rad, 161–0737) with protease and phosphatase inhibitors (Fisher Scientific, 784442). Samples were heated at 95° Celsius for 5 min, separated by SDS-PAGE, and transferred to PVDF membrane. After blocking non-specific proteins using bovine serum albumin (Fisher Scientific, BP1605100) the membranes were stained with antibody for AMPK (Cell Signaling Technology, 5831), phospho-AMPK (Cell Signaling Technology, 2535), PPARγ (Proteintech, 16643-1-AP) or β-actin (Abcam, ab213262) used as a loading control. After washing the blots, immune specific complexes were detected with HRP-conjugated goat anti-rabbit antibody (Jackson Laboratories, 1110335045) and SuperSignal West Pico Substrate (Thermos Fisher Scientific, 34080). Blots were scanned with a ChemiDoc MP Imaging System (Bio-Rad, 12003154) and band intensities evaluated with Image Lab (Bio-Rad).

Table 1
Primers used for qRT-PCR.

Gene Name	Forward primer	Reverse primer
Prkaa2	GTCATCTCAGGAAGGCTGTATG	GTGCTCATCATCGAAAGGGA
Pparg	AGCATTTCTGCTCCACACTAT	GGTTCTACTTTGATCGCACTTTG
Fasn	AGACCCGAACTCCAAGTTATTC	GCAGCTCCTTGTATACTTCTCC
Scd1	GGTGATGTTCCAGAGGAGAATG	CAACCCACGTGAGAGAAGAAG
Fabp4	GCTCCTCCTCGAAGGTTTAC	CCCACTCCCACTTCTTTCAT
Atf5	GCTCGTAGACTATGGGAAACTC	CAGAGAAGCCGTCACCTG
Hspa9	GCAGTGGTTGGTATTGATTTGG	AGCATTCTCCAGGACCTTTG
Hspa5	CTGTGGTACCCACCAAGAAG	GGGTCGTTCACCTTCATAGAC
Ddit3	TCCGAGAGCTGCTCAGTTA	GACTGGACACTTGGCATCAATA
Trib3	GGACAAGATGCGAGCTACAC	GACTGGACACTTGGCATCAATA
Ndufa1	CACTGCGTACATCCACAAATTCA	CCAGGCCCTTGGACACATA
Cox8b	GCCATAGTCGTTGGCTTCAT	CTCAGGGATGTGCAACTTCAT
Sdha	CTCTGAGGGATTGGCTTGATTA	AGGCTCAGCTTGCTCTTATAC
Tbp	CCTCACCAACTGTACCATCAG	GGGATTCAGGAAGACCACATAG
Polr2a	GCCTGAACTTAAGGAGCTTATC	CTCGTGCAGATTGACCTAACA

2.6. Measuring mitochondrial mass and mitoROS production

HL-1 cells were exposed to room air or hyperoxia for 36 h before 50 nM MitoTracker Green and 5 mM MitoSOX Red (ThermoFisher Scientific, M7514 and M36008) were added to the culture media. Cells were incubated at 37° Celsius for 15 min before the medium was replaced with Hank's balanced salt solution (HBSS). Cells were incubated at 37° Celsius for another 15 min and imaged with a Celigo Imaging Cytometer (Nexcelom, 200-BFFL-5C) to determine the average mean intensities of MitoTracker and MitoSOX staining in each well. The mean intensity of MitoSOX staining was divided by that of MitoTracker staining to normalize mitoROS to mitochondrial mass.

2.7. Statistical analysis

Data was analyzed with JMP12 (SAS Institute, Cary NC) and graphed with Prism 10 (GraphPad Software, Boston MA). Univariant studies with 2 groups were judged using unpaired 2-tailed *t* tests. Bonferroni multiple t-tests were used to correct repeated measurements. Univariant studies with 3 or more groups were judged using one-way ANOVA with Tukey post hoc tests. Multivariant studies were judged using two-way ANOVA with Sidak multiple comparison tests. The Bland-Altman method was used to determine if samples had equal or unequal variance. In all experiments, $P < 0.05$ was considered significant.

3. Results

3.1. Hyperoxia activates AMPK signaling in mouse atrial cardiomyocytes

Affymetrix arrays were previously used to show that hyperoxia suppresses expression of *Fasn*, *Scd1*, and many other genes controlling fatty acid metabolism in atrial cardiomyocytes isolated from PND4 mice [20]. A Kyoto Encyclopedia of Genes and Genomes (KEGG) analysis of

this dataset implicated AMPK, insulin, glucagon, and PPAR signaling as potential mediators of hyperoxia on fatty acid gene expression (Fig. 1A). AMPK signaling was most intriguing since it had the highest probability score and was shown to directly inhibit sterol response element binding protein (SRBP), a transcriptional master regulator of *de novo* fatty acid synthesis genes [27]. The levels of phosphorylated AMPK (*p*-AMPK) and total AMPK were thus examined by western blotting in lysates of left atria isolated from PND4 mice exposed to room air or hyperoxia. It revealed hyperoxia increased *p*-AMPK, but not total AMPK protein or β-actin (Fig. 1B and C). Hyperoxia also increased *p*-AMPK in mouse atrial cardiomyocyte HL-1 cell line (Fig. 1C and D).

To determine whether AMPK activation would replicate the effects of hyperoxia, HL-1 cells were cultured with 0, 0.5, 1.0, and 2.0 mM of the AMPK activating compound 5-aminoimidazole-4-carboxamide ribonucleotide (AICAR) for 36 h. Western blotting revealed AICAR stimulated *p*-AMPK in a dose-dependent manner (Fig. 2A and B). To determine if AMPK activation mimics the effects of hyperoxia on the expansion of atrial cardiomyocytes, HL-1 cells were cultured in increasing doses of AICAR and exposed to room air for 48 h. Cells were collected every 12 h, stained with the permeable DNA dye Hoechst 33342 and quantified using an imaging cytometer. Exposing HL-1 cells to 0.5 and 1.0 mM AICAR inhibited growth while 2.0 mM AICAR reduced survival with loss of cells seen by 48 h (Fig. 2C).

To determine if AMPK activation would reproduce the effects of hyperoxia on fatty acid synthesis genes, HL-1 cells were treated with 0, 0.5, 1.0, and 2.0 mM AICAR and cultured in room air for 48 h qRT-PCR revealed AICAR did not affect *Fasn*, it inhibited *Scd1* and fatty acid binding protein 4 (*Fabp4*), a gene promoting fatty acid uptake and storage that is inhibited by hyperoxia (Fig. 2D–F). AMPK activation thus replicates the effects of hyperoxia on fatty acid synthesis and cell growth in room air.

The role of AMPK in mediating the effects of hyperoxia were tested by transfected HL-1 cells with siRNAs targeting *Prkaa2*, the predominant catalytic subunit of AMPK in the heart or non-targeting (NT) siRNA. The cells were then cultured in room air or hyperoxia for 48 h. Hyperoxia reduced *Prkaa2* mRNA by around 20 % which was further suppressed by siRNAs targeting its expression (Fig. 3A). HL-1 cells cultured in room air and transfected with *Prkaa2* siRNA grew slower than NT controls (Fig. 3B), a result that was unexpected since activating AMPK using AICAR also inhibited their proliferation. Silencing *Prkaa2* failed to restore proliferation of cells exposed to hyperoxia and unexpectedly increased the toxicity of hyperoxia after 24 h (Fig. 3C).

To evaluate the effects of *Prkaa2* knockdown on the hyperoxia-dependent suppression of fatty acid synthesis genes, cells were treated with *Prkaa2* and NT siRNA and exposed to hyperoxia or room air for 48 h before RNA was extracted for qRT-PCR. Suppressing *Prkaa2* increased *Fasn, Scd1, and Fabp4* expression in HL-1 cells cultured in room air but did not prevent hyperoxia from inhibiting *Fasn, Scd1, or Fabp4* expression (Fig. 3D–F). Taken together, these findings reveal hyperoxia activates AMPK, but AMPK is not required for hyperoxia to inhibit cardiomyocyte proliferation or suppress expression of fatty acid synthesis genes.

3.2. *Hyperoxia stimulates PPAR γ transcriptional activity*

In addition to AMPK, the PPAR-family of nuclear hormone receptors

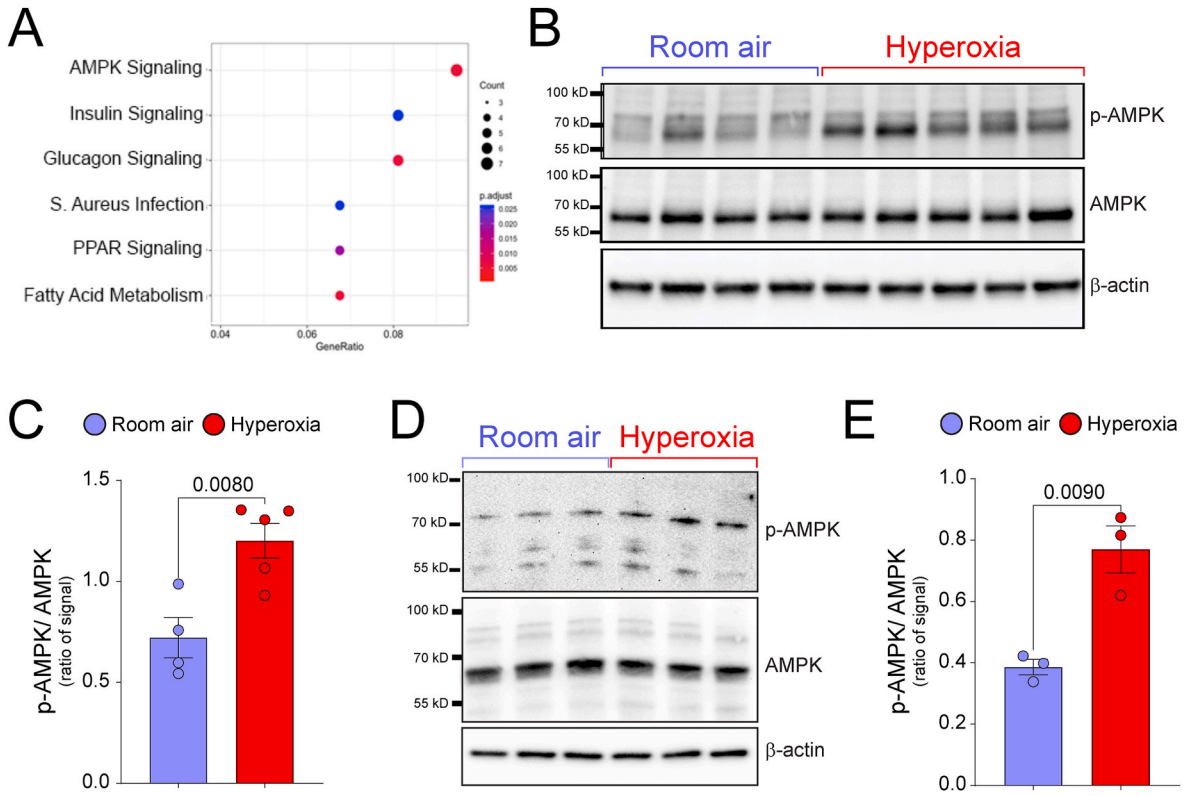

Fig. 1. Hyperoxia increases AMPK activity in atrial cardiomyocytes. (**A**) KEGG analysis of left atrial cardiomyocytes isolated from neonatal mice exposed to room air or hyperoxia between PND0-4. The size of the dot reflects number of genes within a pathway while color reflects statistical significance relative to room air. (**B**) Western blot of lysates from the left atria of mice exposed to room air or hyperoxia from PND0-4 probed for *p*-AMPK, total AMPK, and β-actin. Each lane represents the left atrium of a single heart. (**C**) Band intensities of *p*-AMPK and total AMPK were determined by Image Lab and graphed as the mean fold change ± SD with individual samples represented as circles. (**D**) The expression of *p*-AMPK, total AMPK, and β-actin was detected by Western blot in HL-1 cells cultured in room air or hyperoxia for 48 h. (**E**) Band intensities were determined with Image Lab and graphed as the ratio of *p*-AMPK to total AMPK with independent replicates shown as circles. (**C, E**) P values are the results of student's t-tests. (For interpretation of the references to color in this figure legend, the reader is referred to the Web version of this article.)

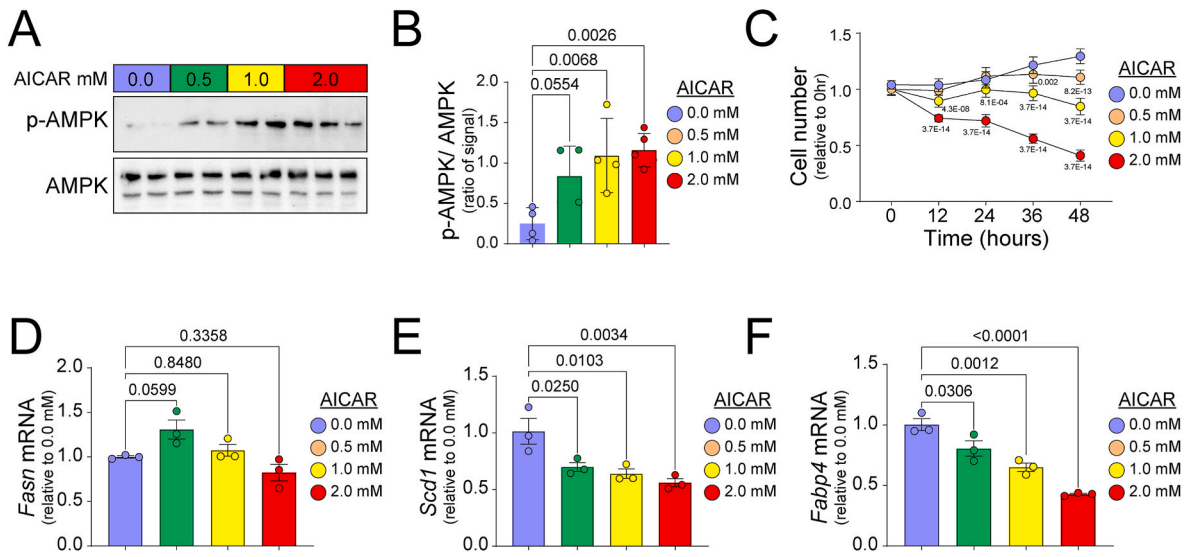

Fig. 2. AICAR mimics the effects of hyperoxia on HL-1 cells. (**A**) Western blot of *p*-AMPK, total AMPK, and β-actin in HL-1 cells cultured in 0 (blue), 0.5 (green), 1.0 (yellow), and 2.0 (red) mM AICAR for 36 h. (**B**) The ratio of *p*-AMPK to total AMPK was graphed as mean fold change over room air ± SD with individual values as circles. (**C**) Mean number of HL-1 cells cultured in 0, 0.5, 1.0, and 2.0 mM AICAR per well ± SD before (0 h) and 12, 24, 36 and 48 h after treatment. (**D-F**) results of qRT-PCR for *Fasn* (**D**), *Scd1* (**E**), and *Fabp4* (**F**) mRNA in cells cultured with 0–2.0 mM AICAR for 36 h. Data is graphed as mean fold change ± SD of control cells without AICAR with individual values shown as circles. P values are the results of one-way with Tukey post hoc test (**B, D, E, F**) or two-way ANOVA with Sidak multiple comparison test (**C**). (For interpretation of the references to color in this figure legend, the reader is referred to the Web version of this article.)

were of interest due to their critical roles in balancing mitochondrial β-oxidation with lipid synthesis and storage. While cardiomyocytes express PPARα and PPARβ/δ, PPARγ promotes lipid synthesis and storage in the heart and induces fatty acid synthesis genes when overexpressed in the cardiomyocytes of adult mice [28,29]. PPARγ was identified by western blotting of left atrial lysates isolated from PND4 mice, but its expression was not significantly affected by neonatal hyperoxia (Fig. 4A). Hyperoxia also did not affect expression of PPARγ in HL-1 cells (Fig. 4B). The level of PPARγ protein is therefore unaffected by hyperoxia *in vivo* and *in vitro*.

Since the KEGG analysis of left atrial cardiomyocytes indicates hyperoxia affects expression of PPARγ targets, we investigated whether hyperoxia affects PPARγ transcriptional activity in HL-1 cells using a PPARγ responsive firefly luciferase reporter *PPRE-LUC* and a constitutive *Renilla* luciferase reporter used to control for transfection efficiency. Intriguingly, PPRE-Luc activity was approximately 2-fold higher in cells exposed to hyperoxia for 48 h than control exposed to room air (Fig. 4C). To more specifically test how hyperoxia affects PPARγ activity, cells were co-transfected with luciferase reporters and PPARγ expression vector and cultured in the absence or presence of 10 mM of the PPARγ agonist rosiglitazone. While PPARγ overexpression and rosiglitazone separately increased PPRE-Luc activity by approximately 2-fold in cells exposed to room air, combined treatment led to a nearly 10-fold increase in PPRE-Luc activity (Fig. 4D). Hyperoxia consistently increased PPRE-Luc activity approximately 2-fold under all conditions (i.e., ~20 fold in PPARγ overexpressing cells with rosiglitazone), indicating that is enhances ligand-dependent PPARγ activity. As final evidence that hyperoxia increases PPARγ transcriptional activity, PPRE-Luc activity was evaluated when PPARγ expression was effectively silenced using siRNA (Fig. 4E). As expected, silencing PPARγ expression reduced PPRE-Luc activity approximately 2-fold lower compared to NT siRNA treated cells in room air (Fig. 4F). Moreover, silencing PPARγ blunted the approximately 3-fold increases in PPRE-Luc observed in cells exposed to hyperoxia. The PPRE-Luc activation caused by hyperoxia is thus likely due to enhanced PPARγ activity.

3.3. Hyperoxia uses PPARγ to inhibit HL-1 cell proliferation and survival

To determine how increased PPARγ activity affected the proliferation, survival, and fatty acid gene expression of atrial cardiomyocytes, HL-1 cells transfected with PPARg or NT siRNA were plated at equal density and grown in room air or hyperoxia for 48 h. Cells transfected with PPARg and NT siRNA grew at equal rates throughout the 48-h period in room air (Fig. 5A). While PPARg and NT siRNA treated cells initially grew at equal rates in hyperoxia, PPARγ-deficient HL-1 cells continued to expand between 24 and 36 h before declining while NT siRNA treated control cells began to decline sooner. Silencing PPARγ restored proliferation as defined by increased 5-ethynyl-2′-deoxyuridine (EdU) used to label cells in S-phase (Fig. 5B). It also reduced cell death as defined by staining with the cell permeable DNA dye Hoechst and dye propidium iodide (PI), a vital dye that labels the DNA of dying cells that have lost membrane integrity (Fig. 5C). Silencing PPARγ also increased *Fabp4* expression in room air and blocked the suppression of *Scd1* and *Fabp4* in hyperoxia (Fig. 5C–E). It had no effect on expression of *Fasn*, indicating hyperoxia represses *Fasn* though other effectors. Together, these finding suggest PPARγ mediates many of the effects of hyperoxia on cardiomyocyte proliferation, survival, and expression of fatty acid genes.

3.4. PPAR γ knockdown reduces mitoROS and mitochondrial mass

Treating neonatal mice with the mitochondrially targeted antioxidant MitoTEMPO alleviated the inhibitory effects of neonatal hyperoxia on atrial cardiomyocyte proliferation, suggesting mitoROS mediates the anti-proliferative effects of hyperoxia on these cells [21]. To evaluate the effects of hyperoxia on mitoROS levels, cells transfected with *Pparg* and NT siRNA were exposed to hyperoxia for 48 h and co-stained with the mitoROS indicator MitoSOX Red, the mitochondrial mass indicator mitoTracker green, and DNA dye Hoechst 33342 (Fig. 6A). Hyperoxia increases MitoSOX and deceased tracker green staining, which when graphed together reflected a net increase in mitoROS per dish (Fig. 6B–D). Interestingly, the ratio of MitoSOX to Hoechst staining was lower in PPARγ siRNA treated cells compared to NT transfected control cells, regardless of whether cells were in room air or hyperoxa.

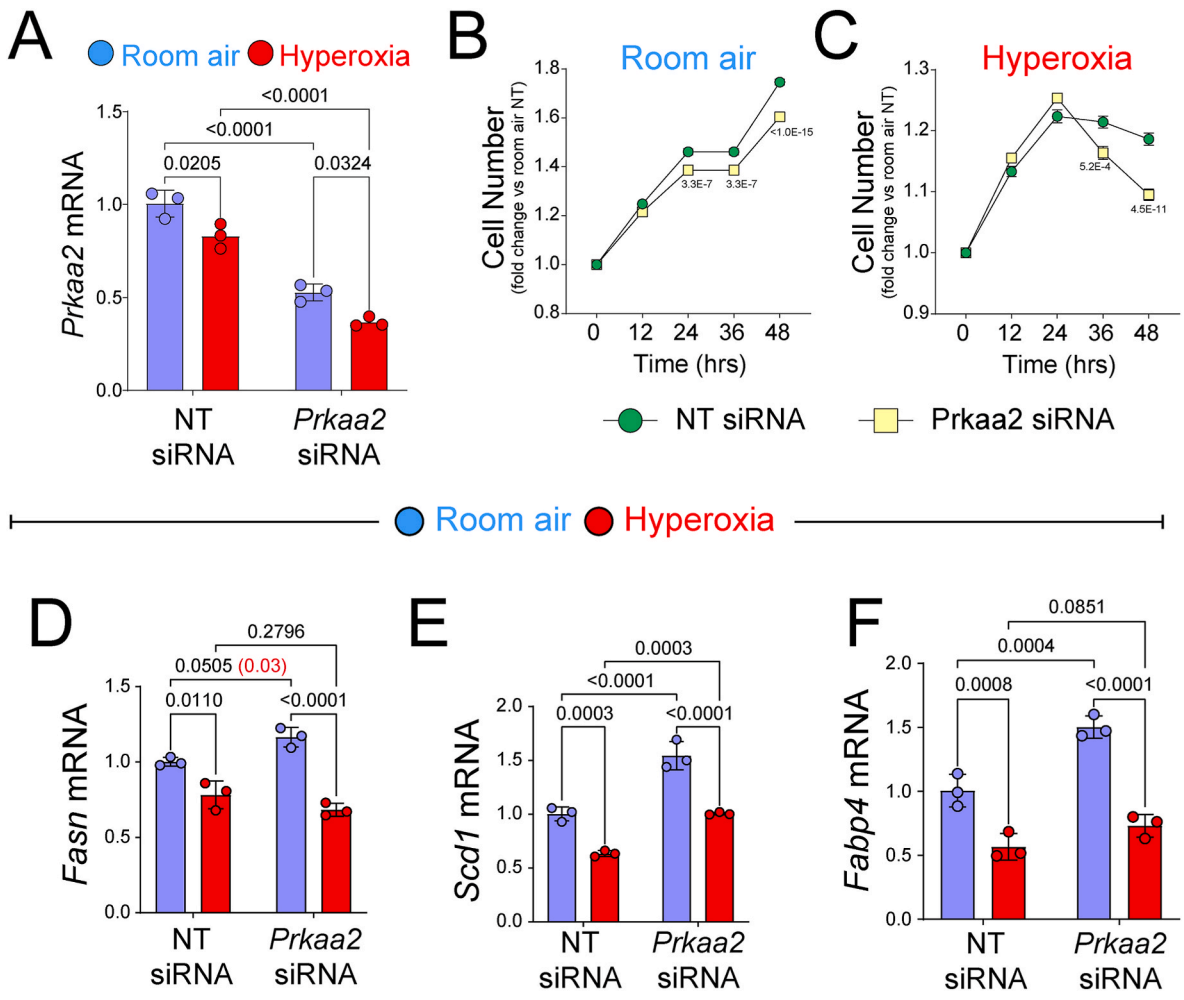

Fig. 3. Silencing AMPK does not preserve HL-1 cell growth or fatty acid synthesis gene expression in hyperoxia. (**A**) HL-1 cells were transfected with *Prkaa2* targeting or non-targeting (NT) control siRNA, allowed to recover for 24 h, and exposed to room air or hyperoxia for 48 h. *Prkaa2* mRNA was then examined by qRT-PCR and graphed as fold change ± SD relative to NT cells in room air. (**B, C**) HL-1 cells transfected with *Prkaa2* or NT siRNA were plated at equal density, exposed to room air (**B**) or hyperoxia (**C**) for 48 h, and counted. Graphs show mean numbers of cells per well ± SD after 0, 12, 24, 36, and 48 h of exposure expressed as fold changes relative to 0 h. (**D-F**) HL-1 cells treated with *Prkaa2* or NT siRNA were exposed to room air or hyperoxia for 48 h. Expression of *Fasn* (**D**), *Scd1* (**E**) and *Fabp4* (**F**) was examined by qRT-PCR. Data is expressed as mean fold change ± SD of control cells without AICAR. Circles show individual samples. P values in black type are the results of two-way ANOVA with Sidak multiple comparison tests. P value in red type in D is the result of a one-way ANOVA with Tukey's *post hoc* test. (For interpretation of the references to color in this figure legend, the reader is referred to the Web version of this article.)

Moreover, normalizing the intensity of MitoSOX staining to MitoTracker indicated the decreased mitoROS in PPARγ deficient cells in room air could be explained by reduced mitochondrial mass (Fig. 6D).

3.5. PPARγ knockdown blunts the mitochondrial unfolded protein response

Since PPARγ did not impact mitoROS we investigated whether it impacted mitochondrial stress signaling. QRT-PCR revealed hyperoxia increases expression of mitochondrial stress responsive transcription factor activating transcription factor 5 (*Atf5*), and the mitochondrial heat shock protein heat shock family A member 9 (*Hspa9*) were upregulated in NT siRNA treated control cells that were exposed to hyperoxia relative to the levels in those exposed to room air (Fig. 6E and F). In contrast, the endoplasmic reticulum (ER) localized chaperone heat shock protein family A member 5 (*Hspa5*), which is activated by unfolded proteins in the ER, was unaffected (Fig. 6G). DNA damage inducible transcript 3 (*Ddit3*), and its downstream effector tribble pseudo kinase 3 (*Trib3*) were also upregulated in control cells exposed to hyperoxia relative those exposed to room air (Fig. 6H and I). Intriguingly, the hyperoxia induced expression of *Atf5*, *Hspa9*, *Ddit3*, and *Trib3* was either blocked or attenuated in cells that were transfected with *Pparg* siRNA relative to NT siRNA treated controls, indicating hyperoxia induces mitoUPR genes through a PPARγ dependent mechanism.

3.6. PPARγ knockdown prevents changes in mitochondrial function and gene expression

The upregulation of mitoUPR genes depends on PPARγ suggesting PPARγ may be required for hyperoxia to disrupt mitochondrial respiration in atrial cardiomyocytes. To test this hypothesis, HL-1 cells were transfected with either NT or *Pparg* siRNA and exposed to room air or hyperoxia for 48 h. Cells were subsequently replated at equal density in unbuffered basal DMEM containing 2.5 mM glucose, 1 mM pyruvate, 1 mM glutamine, and 1 mM carnitine. Oxygen consumption rates (OCR) were measured with a Seahorse™ xFe96 Bioanalyzer, before and after sequential addition of 1.0 μM oligomycin A, 0.25 μM FCCP, and 0.5 μM rotenone combined with 0.5 μM actinomycin A (Fig. 7A). Hyperoxia did not alter basal OCR in NT siRNA-treated cells (Fig. 7B). However, while basal OCR in *Pparg* siRNA-treated cells was higher than in NT siRNA-treated cells in room air, hyperoxia reduced basal OCR in PPARγ-deficient cells to levels comparable to those of room air-exposed NT siRNA-

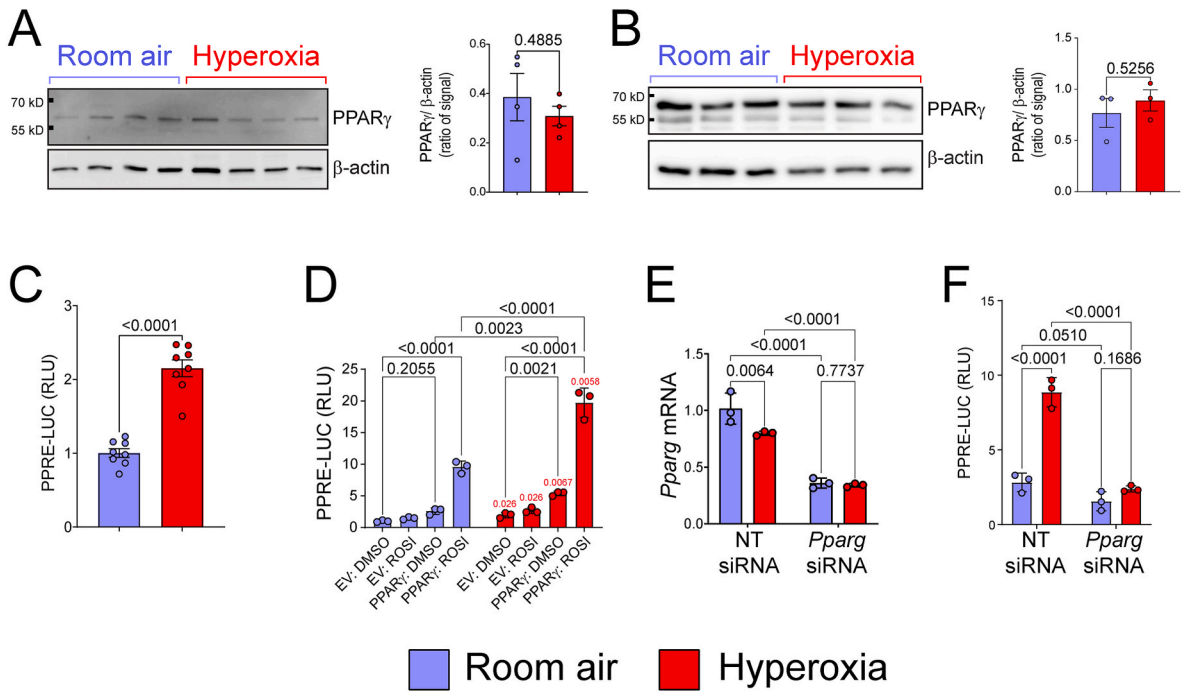

Fig. 4. Hyperoxia increases PPARγ transcriptional activity. (A) Western blotted lysates of left atria from mice exposed to room air or hyperoxia from PND0-4 probed for PPARγ and β-actin. Each lane is a single left atrium. Band intensities were determined with Image Lab and graphed as mean fold change ± SD. (**B**) Western blotted lysates of HL-1 cells exposed to room air or hyperoxia for 48 h probed for PPARγ and β-actin. Band intensities were determined with Image Lab and graphed as mean fold change ± SD. (**C**) HL-1 cells transfected with PPRE-Luc and *Renilla*-Luc were exposed to room air or hyperoxia for 48 h. Relative light units (RLUs) of PPRE-Luc were divided by those of *Renilla*-Luc to normalize for transfection efficiency. Graph shows mean fold change relative to room air ± SD. (**D**) HL-1 cells transfected with PPRE-Luc, *Renilla*-Luc and either empty or PPARγ expression vector and treated with 10 μM rosiglitazone or vehicle (DMSO), were exposed to room air or hyperoxia for 48 h. Graphs show mean fold change in the ratio of RLUs for PPRE-Luc to *Renilla*-Luc relative to empty vector controls with DMSO in room air ± SD. (**E**) Pparγ mRNA was examined by qRT-PCR in HL-1 cells transfected with *Pparg* targeting or NT siRNA and exposed to room air or hyperoxia for 48 h. Graph shows mean fold change relative to NT controls in room air ± SD. (**F**) HL-1 cells transfected with PPRE-Luc, *Renilla*-Luc and either PPARγ or NT siRNA were exposed to room air or hyperoxia for 48 h. Graph shows mean fold change in the ratio of RLUs for PPRE-Luc to *Renilla*-Luc relative to NT controls in room air ± SD. Circles in all graphs show individual samples. P values are the results of student's t-tests (**A-C**) or two-way ANOVA with Sidak multiple comparison tests (**D-F**). Numbers in red above data for hyperoxia exposed cells are adjusted P values from t-tests corrected for multiple comparisons with the Holm Sidak method. (For interpretation of the references to color in this figure legend, the reader is referred to the Web version of this article.)

treated cells. In contrast, ATP-linked OCR was lower in NT siRNA-treated cells after hyperoxia exposure compared to room air (Fig. 7C). ATP-linked OCR was similar between room air-exposed *Pparg* and NT siRNA-treated cells, but PPARγ-deficient cells showed a higher OCR than NT siRNA-treated cells after hyperoxia exposure. ATP-linked OCR in *Pparg* siRNA cells was equivalent under both room air and hyperoxia conditions, indicating that hyperoxia's impact on mitochondrial function is PPARγ-dependent. Hyperoxia did not affect maximum (Fig. 7D) or non-mitochondrial OCR (Fig. 7E).

Given previous studies implicating PPARγ in mitochondrial biogenesis, we examined the expression of genes encoding components of the electron transport chain using qRT-PCR. Despite the loss of ATP-linked respiration in hyperoxia-exposed cells compared to controls, mRNA levels for mitochondrial Complex I protein NADH: ubiquinone oxidoreductase A1 (*Ndufa1*) (Fig. 7F), Complex IV protein Cytochrome *c* oxidase subunit 8B (*Cox8b*) (Fig. 7G), and Complex II protein succinate dehydrogenase subunit A (*Sdha*) (Fig. 7H) were upregulated in NT siRNA-treated cells that were exposed to hyperoxia relative to room air-exposed cells. In contrast, hyperoxia did not affect *Ndufa1* or *Cox8b* levels in *Pparg* siRNA-treated cells. Although hyperoxia increased *Sdha* expression in PPARγ-deficient cells, the magnitude of this increase was less than that observed in NT siRNA-treated cells.

3.7. PPARγ inhibition increases atrial cardiomyocyte proliferation and survival in mice exposed to neonatal hyperoxia

Since silencing PPARγ increased proliferation and survival in hyperoxia, we reasoned treating mice with the PPARγ inhibitor GW9662 while they are exposed to hyperoxia may preserve the proliferation and survival of left atrial cardiomyocytes *in vivo*. To confirm GW9662 and PPARγ siRNA cause similar increases in the proliferation and survival of HL-1 cells in hyperoxia, cells were plated at equal densities in media with 50 nM GW9662 or DMSO to control for vehicle. One plate was fixed at zero hours and the rest were exposed to room air or hyperoxia for 36 h before being stained and counted. Hyperoxia reduced the growth of cells in DMSO containing media but did not affect the growth of cells treated with GW9662 (Fig. 8A). Additional cells were treated with GW9662 or DMSO, exposed to room air or hyperoxia for 36 h and cultured in EdU containing media for 30 min to label cells in S-phase. While hyperoxia reduced the fraction of EdU labeled cells in both GW9662 and DMSO (Fig. 8B), EdU labeled more GW9662 treated cells than control cells in hyperoxia. GW9662 and DMSO treated cells were also stained with PI after being exposed to hyperoxia or room air for 36 h to determine if GW9662 increased the survival of HL-1 cells in hyperoxia. Hyperoxia increased the numbers of PI positive cells in GW9662 and DMSO, but far fewer GW9662 treated cells were PI positive than controls in hyperoxia (Fig. 8C). Together, these data indicate GW9662 and PPARγ knockdown have similar effects on restoring HL-1 cell proliferation and survival in hyperoxia.

Since PPARγ is required for hyperoxia to inhibit HL-1 cell proliferation and survival, we sought to determine if PPARγ inhibition would increase the proliferation and survival of atrial cardiomyocytes in neonatal hyperoxia exposed mice. Newborn mice were exposed to room air or hyperoxia from PND0-4 as described but injected with 5 μg/mg of

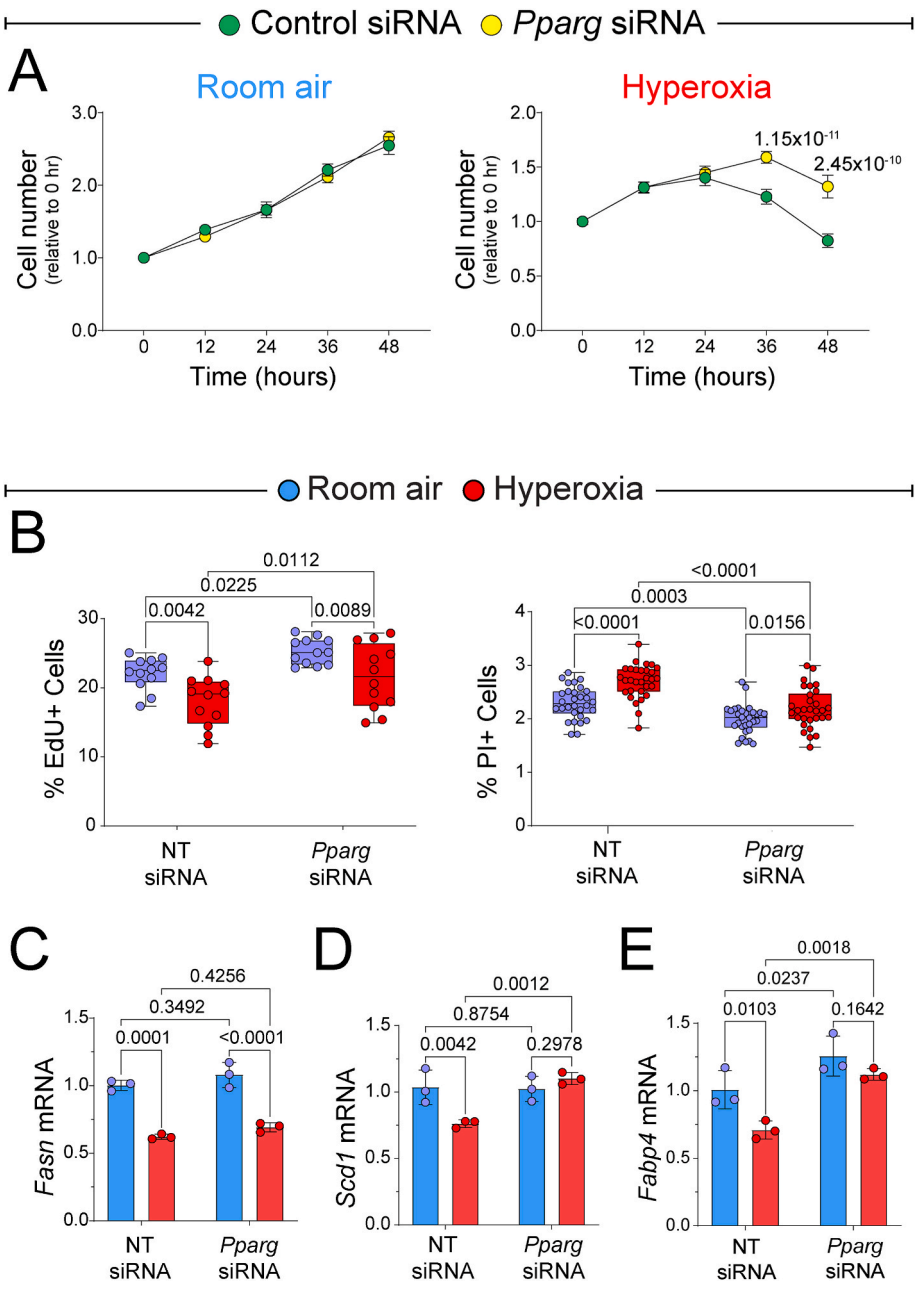

Fig. 5. PPARγ contributes to the effects of hyperoxia on cell proliferation and survival. (**A**) HL-1 cells transfected with *Pparg* or NT siRNA were exposed to room air (left) or hyperoxia (right) for 48 h. Graphs show fold changes in mean numbers of *Pparg* and NT siRNA transfected cells at 12, 24, 36, and 48 h relative to cell numbers at 0 h ±SD. **B**) HL-1 cells transfected with *Pparg* or NT siRNA were exposed to room air or hyperoxia for 36 h and then labeled with EdU or propidium iodide (PI). Box plots show median percentages of EdU (left), and PI (right) labeled cells with 2nd and 3rd quartiles, whiskers show range of values. (**C-E**) HL-1 cells transfected with *Pparg* or NT siRNA were exposed to room air or hyperoxia for 48 h before the levels of *Fasn* (**C**), *Scd1* (**D**) and *Fabp4* (**E**) mRNA were evaluated by qRT-PCR. Graph shows mean fold changes relative to NT controls in room air ± SD. (**B-E**) Circles show individual samples. P values are the results of two-way ANOVA with Sidak multiple comparison tests.

GW9662 in corn oil or corn oil alone to control for vehicle. Hearts were collected on PND4 and fixed for histological sectioning. Sections were co-stained for the proliferation marker Ki67 and the cardiomyocyte marker TNNI3. Hyperoxia reduced the fraction of TNNT2 labeled cardiomyocytes in the left atria of vehicle treated mice that expressed Ki67 relative to controls (Fig. 8D and E). While the fraction of cardiomyocytes in the left atria that expressed Ki67 were equivalent in vehicle and GW9662 treated mice in room air, more left atrial cardiomyocytes expressed Ki67 in GW9662 treated mice than vehicle treated controls in hyperoxia. Hyperoxia also failed to increase the fraction of Ki67 expressing cardiomyocytes in the left atria of GW9662 treated mice as it did in vehicle treated controls. To determine if PPARγ inhibition affects the survival of atrial cardiomyocytes in mice exposed to neonatal hyperoxia, sections were co-stained with antibodies for the cleaved, active form of Caspase3 (cl-Casp3) and TNNI3. More TNNI3 labeled cardiomyocytes expressed cl-Casp3 in vehicle-treated mice that were exposed to neonatal hyperoxia than vehicle treated mice exposed to room air (Fig. 8F and G). Fewer cardiomyocytes expressed cl-Casp3 in GW9662 treated mice than vehicle treated controls in both room air and hyperoxia. Moreover, hyperoxia did not affect the numbers of cl-Casp3 labeled cardiomyocytes in the left atria of GW9662 treated mice as it did in vehicle controls. These cumulative data indicate PPARγ inhibition

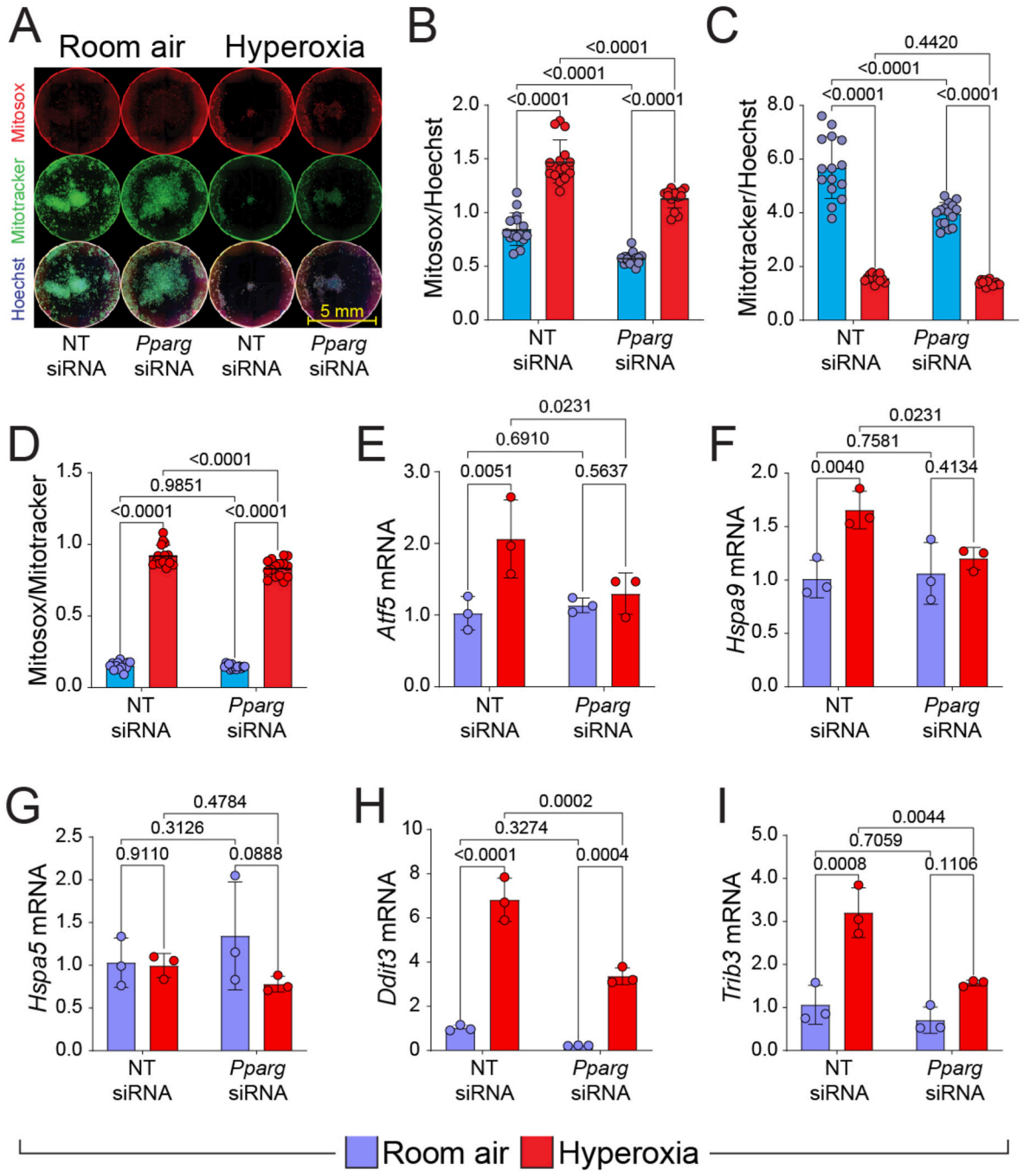

Fig. 6. PPARγ contributes to mitoROS production and the activation of mitochondrial stress response genes in hyperoxia. (**A**) Representative images of HL-1 cells transfected with *Pparg* or NT siRNA, exposed to room air or hyperoxia for 48 h, and stained with MitoSOX (Red), MitoTracker (Green), and Hoechst (blue). (**B-D**) Mean intensity of MitoSOX (**B**) and MitoTracker (**C**) staining normalized to Hoechst, or mean intensity of MitoSOX staining normalized to MitoTracker (**D**) ± SD. (**E-I**) HL-1 cells transfected with *Pparg* or NT siRNA were exposed to room air or hyperoxia for 48 h and *Atf5* (**E**), *Hspa9* (**F**), *Hspa5* (**G**), *Ddit3* (**H**) and *Trib3* (**I**) expression examined by qRT-PCR. Graphs show mean fold change in mRNA levels ± SD. (**B–I**) Circles show individual samples and P values are the results of two-way ANOVA with Sidak multiple comparison tests. (For interpretation of the references to color in this figure legend, the reader is referred to the Web version of this article.)

ameliorates the loss of atrial cardiomyocyte proliferation and survival in mice that were exposed to hyperoxia as neonates.

4. Discussion

Growing evidence suggests the supplemental oxygen therapy used to prevent hypoxemia in preterm infants leads to cardiopulmonary disease later in life. While hyperoxia increases mitoROS production and mitochondrially targeted antioxidants can prevent hyperoxia-induced disease, the effects of hyperoxia on the newborn heart that initiate cardiopulmonary disease later in life are poorly understood. The results of the current studies reveal hyperoxia activates AMPK and PPARγ in atrial cardiomyocytes *in vivo* and *in vitro*. While activating AMPK inhibited fatty acid synthesis and expansion of HL-1 atrial cardiomyocytes, hyperoxia still inhibited fatty acid synthesis and the proliferation and survival of HL-1 cells in the absence of AMPK. In contrast,

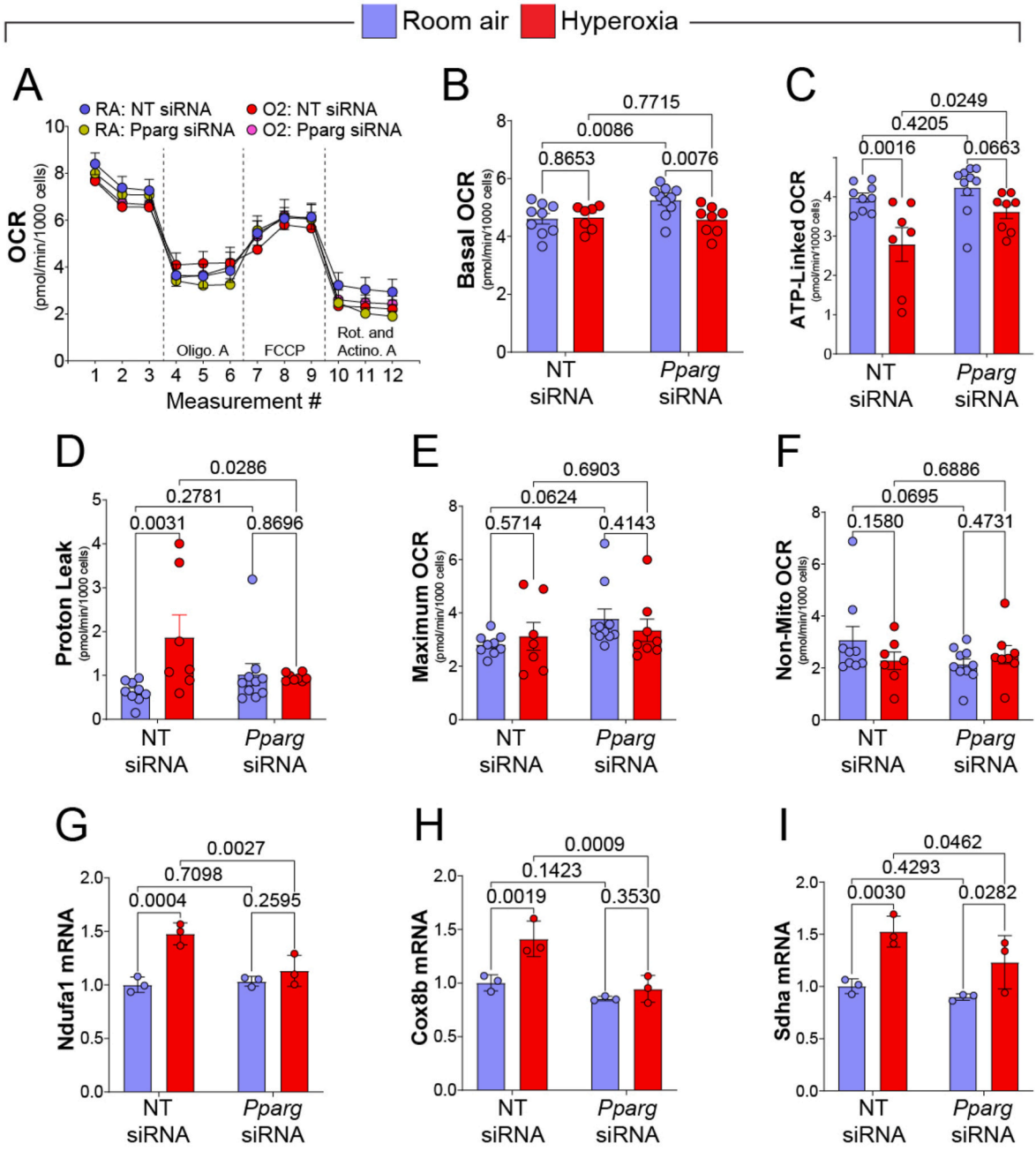

Fig. 7. PPARγ knockdown inhibits hyperoxia-induced changes in mitochondrial function and gene expression in HL-1 cells. (**A**) Time-course of oxygen consumption rate (OCR) in NT (blue, red) and *Pparg* (green, violet) treated cells that were exposed to room air (blue, green) or hyperoxia (red, violet) for 48 h. Circles and error bars represent mean OCR ± SEM in pmol/min/1000 cells. Sample sizes: NT siRNA in room air (N = 9) and hyperoxia (N = 7); Pparg siRNA in room air (N = 10) and hyperoxia (N = 8). (**B–F**) Graphs showing basal OCR (**B**), ATP-linked OCR (**C**), proton leak (**D**), maximum OCR (**E**), and non-mitochondrial OCR (**F**) for NT (left) and *Pparg* siRNA (right) treated cells exposed to room air (blue) or hyperoxia (red). Circles are OCRs of individual wells expressed as pmol/min/1000 cells. Error bars represent SEM. (**E-I**) Relative expression of *Ndfa1* (**E**), *Cox8b* (**F**), and *Sdha* (**G**) compared to NT treated cells in room air. Circles are values from independent replicates. Error bars = SEM. N = 3 for all conditions. (For interpretation of the references to color in this figure legend, the reader is referred to the Web version of this article.)

silencing PPARγ extended the growth of HL-1 cells in hyperoxia, prevented the hyperoxia-dependent inhibition of fatty acid synthesis genes, and reduced the expression of stress-responsive genes in hyperoxia treated cells. Treating mice with the PPARγ inhibitor GW9662 during exposure also alleviated the loss of atrial cardiomyocyte proliferation and survival in hyperoxia exposed mice, suggesting PPARγ inhibitors provide a pharmacological approach for preventing the effects of neonatal hyperoxia on atrial cardiac function.

Pathway analysis of previously published Affymetrix array dataset implicated two critical regulators of lipid metabolism, AMPK and PPARγ, in the inhibition of fatty acid synthesis genes, proliferation, and survival in the atrial cardiomyocytes of neonatal hyperoxia exposed mice [20]. AMPK had the higher probability score and was previously shown to inhibit SREBP, a critical regulator of fatty acid synthesis gene transcription [27]. HL-1 cells were thus first treated with the AMPK activator AICAR to determine if AMPK activation would replicate the effects of hyperoxia on atrial cardiomyocytes in room air. AICAR treatment inhibited both fatty acid synthesis genes and expansion of

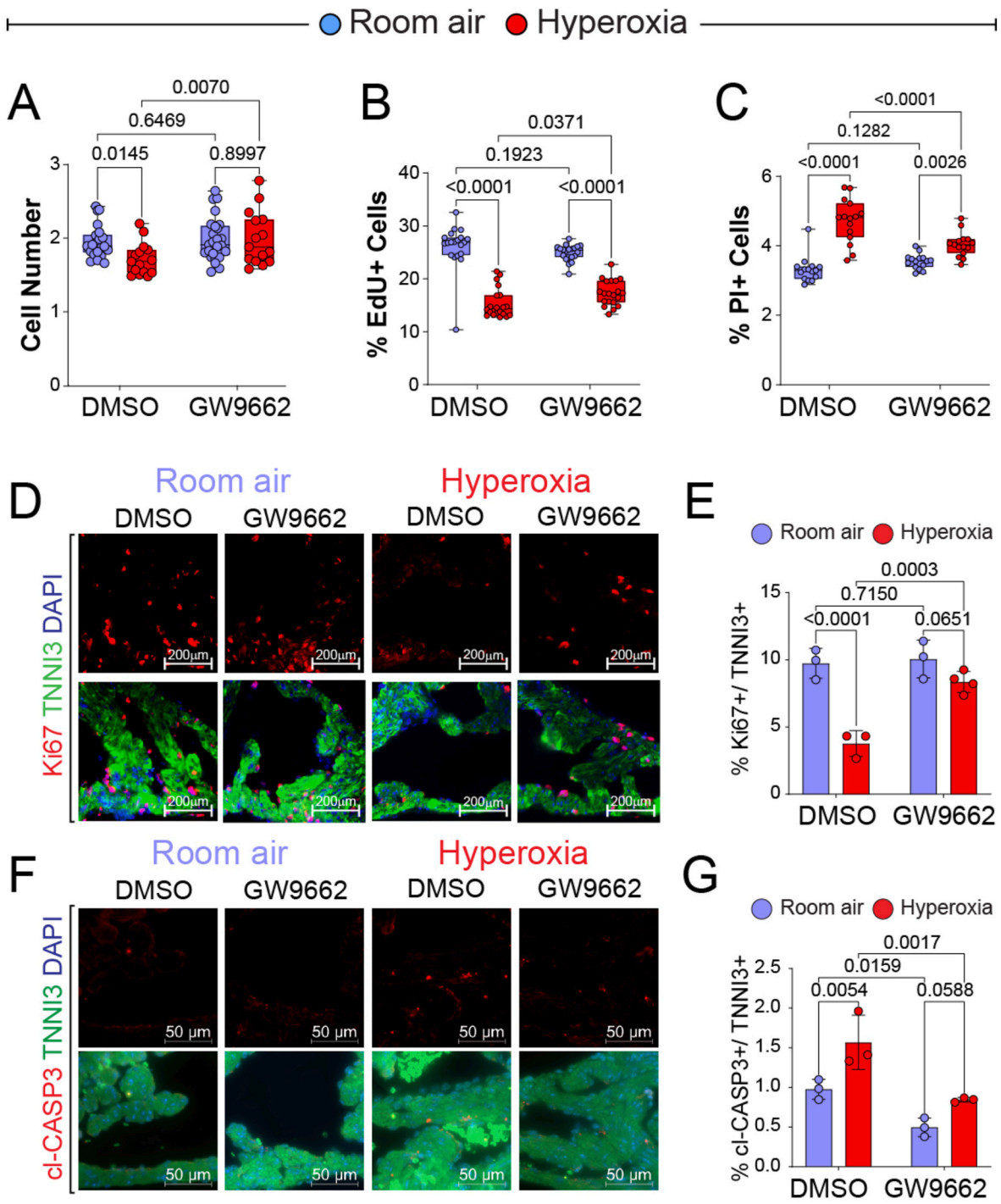

Fig. 8. The PPARγ inhibitor GW9962 preserves atrial cardiomyocyte proliferation and survival in hyperoxia exposed mice. HL-1 cells cultured in 50 μM GW9662 or vehicle (DMSO) were exposed to room air or hyperoxia for 36 h and labeled with EdU or PI. (**A-C**) Box plots show median fold change in cell number relative to 0 h (**A**) or median percentages of EdU (**B**) and PI (**C**) labeled cells with 2nd and 3rd quartiles, whiskers show the range of values. Circle show individual samples (**D-G**) Sections of hearts from PND4 mice that were exposed to room air or hyperoxia from PND0-4 and injected with 5 μg/mg GW9662 or vehicle (corn oil) on PND0 and PND2 stained for Ki-67, TNNI3, and DAPI (**D**) or cleaved caspase 3, TNNI3, and DAPI (**F**). Graphs show mean percentages of Ki67 (**E**) and cl-Caspase3 (**G**) labeled cells ± SD. P values are the results of two-way ANOVA with Sidak multiple comparison tests.

HL-1 cells in room air, consistent with its mediating the effects of hyperoxia. However, *Prkaa2* knockdown did not restore fatty acid synthesis or HL-1 cell growth in hyperoxia. This suggests AMPK may lie downstream in a linear pathway linking hyperoxia, AMPK and fatty acid gene expression. Prior studies have shown that AMPK activity is increased in the hearts, muscles, and livers of *Scd1* knockout mice relative to wild type controls [30–32]. AMPK activation may thus be a downstream consequence hyperoxia suppressing *Scd1* expression. Based on these observations, we conclude AMPK is unnecessary for hyperoxia to inhibit fatty acid synthesis and proliferation or survival of atrial cardiomyocytes. AMPK inhibition is thus unlikely to alleviate the effects of neonatal hyperoxia on the postnatal expansion of atrial cardiomyocyte, demonstrating the dangers of relying solely on mathematical analyses of gene expression data to predict biological causality.

Since PPARγ is essential for adipogenesis and transactivates fatty acid synthesis genes in both differentiating adipocytes and the cardiomyocytes of adult mice [29,33], we initially hypothesized hyperoxia repressed fatty acid synthesis genes via PPARγ inhibition. We were thus surprised to find higher levels of PPARγ activity in hyperoxia treated HL-1 cells than controls. Moreover, PPARγ knockdown increased the proliferation, survival, and expression of fatty acid synthesis genes in hyperoxia treated HL-1 cells relative to NT siRNA transfected controls. Treating mice with the PPARγ inhibitor GW9662 during neonatal hyperoxia exposure similarly prevented the loss of left atrial cardiomyocyte proliferation and survival in the left atrium. Hyperoxia thus causes PPARγ to actively repress fatty acid synthesis genes in atrial cardiomyocytes *in vivo* as well as *in vitro*. Silencing PPARγ also blunted the hyperoxia-dependent expression of mitoUPR genes in HL-1 cells, consistent with data from prior studies showing PPARγ overexpression induced *Ddit3* expression in the cardiomyocytes of adult mice and non-small cell carcinomas [28,34]. Intriguingly, *Ddit3* and *Trib3* both have predicted PPRE sites in their promoters and may thus be direct targets of PPARγ [35]. Taken together, these data suggest hyperoxia causes PPARγ to preferentially activate stress related target genes, but perhaps at the expense of also inhibiting genes required for lipid metabolism and hence expansion of cardiomyocytes.

Our finding that hyperoxia slightly reduces *Pparγ* mRNA but not protein expression suggests it activates PPARγ transcriptional activity through a post-translational change in PPARγ itself or its lipid ligand. mitoROS can initiate the peroxidation of poly-unsaturated fatty acids into 4-Hydroxynonenal (4-HNE) and other reactive products that can act as alternative PPARγ ligands. However, ligands produced by lipid peroxidation are shorter than traditional PPARγ ligands and do not fully engage the ligand binding domain. These ligands thus cause distinct conformational changes that affect cofactor binding and favor the activation of stress responsive PPARγ targets. For example, the non-canonical PPARγ ligand NAL SR1664 activated p53 and promoted apoptosis in xenographs of A549 carcinoma cells treated with carboplatin [36]. PPARγ also bound p53 to coactivate genes involved in the regeneration of damaged endothelial cells and stabilized ataxia telangiectasia mutated (ATM), the kinase that recruits p53 to double stranded DNA breaks [37,38]. Moreover, the lipid peroxidation product 4-hydroxyhexenal (4-HHE) was shown to repress the expression of fatty acid synthesis genes in placental trophoblast cells [39]. These reports suggest lipid peroxidation products may cause PPARγ to inhibit fatty acid synthesis genes during hyperoxia. PPARγ is also a phosphoprotein whose transcriptional activity can be modulated by a variety of serine and threonine phosphorylation [40]. Growth factors like insulin suppress PPARγ transcriptional activity when they stimulate serine phosphorylation of PPARγ via MEK (MAPK/ERK kinase). Similarly, activators of protein kinase A and C suppresses MEK-dependent PPARγ transcriptional activity. Conversely, blocking threonine 166 phosphorylation enhances PPARγ transcriptional activity. Intriguingly, AMPK can phosphorylate and suppress PPARγ transcription, while PPARγ agonists can activate AMPK. Preliminary studies looking at interactions between AMPK and PPARγ during hyperoxia suggest that AMPK might be functioning downstream of PPARγ more than functioning upstream. But why AMPK by itself is not able to regulate fatty acid gene expression remains unclear.

PPARγ knockdown reduced MitoTracker staining in HL-1 cells exposed to room air, consistent with prior reports of it promoting mitochondrial biogenesis [41,42]. Furthermore, the release of mitoROS and mitochondrial proteins into the cytosol were recently shown to be essential for mitoUPR activation [43]. Silencing PPARγ may thus reduce mitoROS by decreasing the numbers of mitochondria that can be oxidatively damaged before cells are exposed to hyperoxia. Alternatively, PPARγ may reduce mitochondrial mass indirectly via its activation of DDIT3, which was shown to inhibit genes encoding components of the electron transport chain [44]. Interestingly, hyperoxia increased expression of the mitochondrial complex proteins NDufa1, Cox8b, and Sdha as it reduced ATP-linked oxygen consumption. Silencing PPARγ during hyperoxia restored ATP-linked oxygen consumption and reduced expression of these mitochondrial complex genes. Thus, the loss of ATP-linked respiration in hyperoxia-exposed cells is not due to reduced transcription of electron transport chain genes. Instead, these genes may be upregulated as a compensatory response to oxidative damage, with PPARγ potentially playing a role in either inducing hyperoxia-related mitochondrial damage or in the subsequent effort to restore homeostasis. Further studies will thus be required to determine whether the hyperoxia-dependent effects of PPARγ on mitochondrial mass and mitoROS are direct or mediated by its transactivation of genes in the mitoUPR pathway.

There are several limitations to our study. Our study used mouse atrial HL-1 cells to identify potential mechanisms by which hyperoxia inhibits proliferation of atrial cardiomyocytes. HL-1 cells were established from a subcutaneous cardiac tumor excised from C57BL/6J mouse expressing SV40 under control of the atrial natriuretic peptide promoter [26]. They express markers of differentiated cardiomyocytes (i.e. Myh6, Actc1, Tnnt2, etc.) but their sarcomeres are not as organized as adult cardiomyocytes and they also proliferate. They also have Ca2+ transients and T-tubules indicative of a more postnatal than embryonic phenotype. Although these cells may reflect a more adult-like phenotype, their loss of proliferation and fatty acid gene expression when exposed to hyperoxia correlates well with how neonatal mouse and human cardiomyocytes respond to hyperoxia [20]. The current study showing that chemical inhibitors of PPARγ restore proliferation of HL-1 cells and neonatal atrial cardiomyocytes of mice exposed to hyperoxia add additional evidence that HL-1 cells are a relevant model. Interestingly, the molecular changes shown in HL-1 cells and left atria are not seen in the ventricle, although hyperoxia has been shown to promote differentiation of ventricular cardiomyocytes when it damages DNA and activates DNA-damage cell cycle checkpoints [13]. Hyperoxia may be doing the same in atrial cardiomyocytes, but their profound loss suggests that atrial cardiomyocytes may be more susceptible to oxidation than ventricular cardiomyocytes. Given that hyperoxia also damages vascular endothelial cells, it will be important to fully understand how different chambers and cells of the heart respond directly to hyperoxia and indirectly when vascular injury affects hemodynamics. Finally, it is important to mention how challenging it is to adequately relate the amount of oxygen given to neonatal mice and HL-1 cells with that given to preterm infants. The preterm lung is normally bathed in amniotic fluid containing less than 1 % oxygen [45]. Thus, birth into air causes hyperoxia. Because the preterm lung is immature, supplemental oxygen and ventilation is often used to prevent tissue hypoxemia. The dose and duration of exposure can vary daily as providers seek to maintain arterial oxygen saturations of 92–94 %. Despite this limitation, cardiomyocyte maturation in newborn mice exposed to hyperoxia mirrors the developmental state of human fetal cardiomyocyte of ~22 weeks suggests that the response to hyperoxia seen in mice and HL-1 cells is likely to be taking place in preterm infants.

In summary, the data herein indicates that PPARγ plays a significant role in the neonatal hyperoxia-dependent inhibition of atrial cardiomyocyte proliferation and survival, raising the question of why this seemingly self-destructive response to oxidative stress has evolved. The inhibition of fatty acid synthesis may reduce the levels of poly-unsaturated fatty acids and limit the formation of lipid peroxidation products that form adducts with proteins and disrupt their functions. Reducing fatty acid synthesis may thus help alleviate oxidative damage. The activation of DNA-damage and mitochondrial UPR genes that cause apoptosis may similarly have evolved as a way of removing damaged cardiomyocytes from the left atrial and pulmonary vein. These responses to hyperoxia may thus initially be adaptive since cardiomyocytes can compensate for their reduced numbers and preserve heart function by undergoing hypertrophic growth. However, the increased stress placed on the remaining cardiomyocytes may cause these cells to lose contractility or die as mice age and thus initiate the development of

diastolic dysfunction and heart failure in adults previously exposed to hyperoxia.

5. Conclusions

We found that hyperoxia inhibits proliferation and survival of atrial cardiomyocytes by activating PPARγ transcriptional activity. PPARγ suppresses the production of fatty acids required for growth and survival of cardiomyocytes while decreasing mitochondrial mass and increasing mitochondrial stress signaling. Dampening the production of potentially toxic oxidized fatty acids during hyperoxia may reflect an adaptive protective response, however, it leads to maladaptive outcome of diastolic dysfunction when these changes impair proper postnatal growth and survival of atrial cardiomyocytes.

CRediT authorship contribution statement

E. David Cohen: Writing – review & editing, Writing – original draft, Methodology, Investigation, Formal analysis, Data curation, Conceptualization. **Kyle Roethlin:** Investigation, Data curation. **Min Yee:** Investigation, Data curation. **Collynn F. Woeller:** Resources, Methodology, Investigation. **Paul S. Brookes:** Writing – review & editing, Resources, Methodology, Formal analysis. **George A. Porter:** Writing – review & editing, Methodology, Formal analysis. **Michael A. O'Reilly:** Writing – review & editing, Writing – original draft, Supervision, Funding acquisition, Formal analysis, Data curation, Conceptualization.

Declaration of competing interest

All authors declare no conflicts of interests.

Data availability

No data was used for the research described in the article.

Acknowledgements

This work was funded in part by National Institutes of Health Grants R01 HL168812 (MAO) and R21 AG070585 (MAO/CFW), R01 HL071158 (PSB), and R01 HL144776 (GAP, Jr). The Center Grant P30 ES001247 supported the animal inhalation facility and tissue-processing core. We thank Dave Chalupa for maintaining the rodent oxygen exposure facility and Andrew McDavid for creating the GO analysis image in Fig. 1A.

References

[1] A.J. Lewandowski, P.T. Levy, M.L. Bates, P.J. McNamara, A.M. Nuyt, K.N. Goss, Impact of the vulnerable preterm heart and circulation on adult cardiovascular disease risk, Hypertension 76 (4) (2020) 1028–1037, https://doi.org/10.1161/HYPERTENSIONAHA.120.15574.

[2] E. Naumburg, L. Soderstrom, Increased risk of pulmonary hypertension following premature birth, BMC Pediatr. 19 (1) (2019) 288, https://doi.org/10.1186/s12887-019-1665-6.

[3] H. Carr, S. Cnattingius, F. Granath, J.F. Ludvigsson, A.K. Edstedt Bonamy, Preterm birth and risk of heart failure up to early adulthood, J. Am. Coll. Cardiol. 69 (21) (2017) 2634–2642, https://doi.org/10.1016/j.jacc.2017.03.572.

[4] K. Risnes, J.F. Bilsteen, P. Brown, A. Pulakka, A.N. Andersen, S. Opdahl, E. Kajantie, S. Sandin, Mortality among young adults born preterm and early term in 4 nordic nations, JAMA Netw. Open 4 (1) (2021) e2032779, https://doi.org/10.1001/jamanetworkopen.2020.32779.

[5] C. Crump, A. Groves, J. Sundquist, K. Sundquist, Association of preterm birth with long-term risk of heart failure into adulthood, JAMA Pediatr. 175 (7) (2021) 689–697, https://doi.org/10.1001/jamapediatrics.2021.0131.

[6] K.N. Goss, K. Haraldsdottir, A.G. Beshish, G.P. Barton, A.M. Watson, M. Palta, N. C. Chesler, C.J. Francois, O. Wieben, M.W. Eldridge, Association between preterm birth and arrested cardiac growth in adolescents and young adults, JAMA Cardiol 5 (8) (2020) 910–919, https://doi.org/10.1001/jamacardio.2020.1511.

[7] A.J. Lewandowski, D. Augustine, P. Lamata, E.F. Davis, M. Lazdam, J. Francis, K. McCormick, A.R. Wilkinson, A. Singhal, A. Lucas, N.P. Smith, S. Neubauer, P. Leeson, Preterm heart in adult life: cardiovascular magnetic resonance reveals distinct differences in left ventricular mass, geometry, and function, Circulation 127 (2) (2013) 197–206, https://doi.org/10.1161/CIRCULATIONAHA.112.126920.

[8] J.G. Bensley, R. De Matteo, R. Harding, M.J. Black, The effects of preterm birth and its antecedents on the cardiovascular system, Acta Obstet. Gynecol. Scand. 95 (6) (2016) 652–663, https://doi.org/10.1111/aogs.12880.

[9] S. Johansson, A. Iliadou, N. Bergvall, T. Tuvemo, M. Norman, S. Cnattingius, Risk of high blood pressure among young men increases with the degree of immaturity at birth, Circulation 112 (22) (2005) 3430–3436, https://doi.org/10.1161/CIRCULATIONAHA.105.540906.

[10] J.R. Patel, G.P. Barton, R.K. Braun, K.N. Goss, K. Haraldsdottir, A. Hopp, G. Diffee, T.A. Hacker, R.L. Moss, M.W. Eldridge, Altered right ventricular mechanical properties are afterload dependent in a rodent model of bronchopulmonary dysplasia, Front. Physiol. 8 (2017) 840, https://doi.org/10.3389/fphys.2017.00840.

[11] A. Datta, G.A. Kim, J.M. Taylor, S.F. Gugino, K.N. Farrow, P.T. Schumacker, S. K. Berkelhamer, Mouse lung development and NOX1 induction during hyperoxia are developmentally regulated and mitochondrial ROS dependent, Am. J. Physiol. Lung Cell Mol. Physiol. 309 (4) (2015) L369–L377, https://doi.org/10.1152/ajplung.00176.2014.

[12] K.N. Goss, S. Kumari, L.H. Tetri, G. Barton, R.K. Braun, T.A. Hacker, M.W. Eldridge, Postnatal hyperoxia exposure durably impairs right ventricular function and mitochondrial biogenesis, Am. J. Respir. Cell Mol. Biol. 56 (5) (2017) 609–619, https://doi.org/10.1165/rcmb.2016-0256OC.

[13] B.N. Puente, W. Kimura, S.A. Muralidhar, J. Moon, J.F. Amatruda, K.L. Phelps, D. Grinsfelder, B.A. Rothermel, R. Chen, J.A. Garcia, C.X. Santos, S. Thet, E. Mori, M.T. Kinter, P.M. Rindler, S. Zacchigna, S. Mukherjee, D.J. Chen, A.I. Mahmoud, M. Giacca, P.S. Rabinovitch, A. Aroumougame, A.M. Shah, L.I. Szweda, H.A. Sadek, The oxygen-rich postnatal environment induces cardiomyocyte cell-cycle arrest through DNA damage response, Cell 157 (3) (2014) 565–579, https://doi.org/10.1016/j.cell.2014.03.032.

[14] J.G. Bensley, L. Moore, R. De Matteo, R. Harding, M.J. Black, Impact of preterm birth on the developing myocardium of the neonate, Pediatr. Res. 83 (4) (2018) 880–888, https://doi.org/10.1038/pr.2017.324.

[15] F. Huyard, C. Yzydorczyk, M.M. Castro, A. Cloutier, M. Bertagnolli, H. Sartelet, N. Germain, B. Comte, R. Schulz, D. DeBlois, A.M. Nuyt, Remodeling of aorta extracellular matrix as a result of transient high oxygen exposure in newborn rats: implication for arterial rigidity and hypertension risk, PLoS One 9 (4) (2014) e92287, https://doi.org/10.1371/journal.pone.0092287.

[16] C. Yzydorczyk, B. Comte, G. Cambonie, J.C. Lavoie, N. Germain, Y. Ting Shun, J. Wolff, C. Deschepper, R.M. Touyz, M. Lelievre-Pegorier, A.M. Nuyt, Neonatal oxygen exposure in rats leads to cardiovascular and renal alterations in adulthood, Hypertension 52 (5) (2008) 889–895, https://doi.org/10.1161/HYPERTENSIONAHA.108.116251. HYPERTENSIONAHA.108.116251 [pii].

[17] M. Yee, R.J. White, H.A. Awad, W.A. Bates, S.A. McGrath-Morrow, M.A. O'Reilly, Neonatal hyperoxia causes pulmonary vascular disease and shortens life span in aging mice, Am. J. Pathol. 178 (6) (2011) 2601–2610, https://doi.org/10.1016/j.ajpath.2011.02.010.

[18] K. de Waal, N. Costley, N. Phad, E. Crendal, Left ventricular diastolic dysfunction and diastolic heart failure in preterm infants, Pediatr. Cardiol. 40 (8) (2019) 1709–1715, https://doi.org/10.1007/s00246-019-02208-x.

[19] N.S. Phad, K. de Waal, C. Holder, C. Oldmeadow, Dilated hypertrophy: a distinct pattern of cardiac remodeling in preterm infants, Pediatr. Res. 87 (1) (2020) 146–152, https://doi.org/10.1038/s41390-019-0568-4.

[20] E.D. Cohen, M. Yee, G.A. Porter Jr., E. Ritzer, A.N. McDavid, P.S. Brookes, G. S. Pryhuber, M.A. O'Reilly, Neonatal hyperoxia inhibits proliferation and survival of atrial cardiomyocytes by suppressing fatty acid synthesis, JCI insight 6 (5) (2021), https://doi.org/10.1172/jci.insight.140785.

[21] M. Yee, E.D. Cohen, W. Domm, G.A. Porter Jr., A.N. McDavid, M.A. O'Reilly, Neonatal hyperoxia depletes pulmonary vein cardiomyocytes in adult mice via mitochondrial oxidation, Am. J. Physiol. Lung Cell Mol. Physiol. 314 (5) (2018) L846–L859, https://doi.org/10.1152/ajplung.00409.2017.

[22] Y.C. Long, J.R. Zierath, AMP-activated protein kinase signaling in metabolic regulation, J. Clin. Invest. 116 (7) (2006) 1776–1783, https://doi.org/10.1172/JCI29044.

[23] M. Ahmadian, J.M. Suh, N. Hah, C. Liddle, A.R. Atkins, M. Downes, R.M. Evans, PPARgamma signaling and metabolism: the good, the bad and the future, Nat. Med. 19 (5) (2013) 557–566, https://doi.org/10.1038/nm.3159.

[24] M. Yee, P.R. Chess, S.A. McGrath-Morrow, Z. Wang, R. Gelein, R. Zhou, D.A. Dean, R.H. Notter, M.A. O'Reilly, Neonatal oxygen adversely affects lung function in adult mice without altering surfactant composition or activity, Am. J. Physiol. Lung Cell Mol. Physiol. 297 (4) (2009) L641–L649, https://doi.org/10.1152/ajplung.00023.2009.

[25] A. Omeragic, N. Kara-Yacoubian, J. Kelschenbach, C. Sahin, C.L. Cummins, D. J. Volsky, R. Bendayan, Peroxisome Proliferator-Activated Receptor-gamma agonists exhibit anti-inflammatory and antiviral effects in an EcoHIV mouse model, Sci. Rep. 9 (1) (2019) 9428, https://doi.org/10.1038/s41598-019-45878-6.

[26] W.C. Claycomb, N.A. Lanson Jr., B.S. Stallworth, D.B. Egeland, J.B. Delcarpio, A. Bahinski, N.J. Izzo Jr., HL-1 cells: a cardiac muscle cell line that contracts and retains phenotypic characteristics of the adult cardiomyocyte, Proc. Natl. Acad. Sci. U. S. A. 95 (6) (1998) 2979–2984.

[27] Y. Li, S. Xu, M.M. Mihaylova, B. Zheng, X. Hou, B. Jiang, O. Park, Z. Luo, E. Lefai, J. Y. Shyy, B. Gao, M. Wierzbicki, T.J. Verbeuren, R.J. Shaw, R.A. Cohen, M. Zang, AMPK phosphorylates and inhibits SREBP activity to attenuate hepatic steatosis and atherosclerosis in diet-induced insulin-resistant mice, Cell Metabol. 13 (4) (2011) 376–388, https://doi.org/10.1016/j.cmet.2011.03.009.

[28] N.H. Son, T.S. Park, H. Yamashita, M. Yokoyama, L.A. Huggins, K. Okajima, S. Homma, M.J. Szabolcs, L.S. Huang, I.J. Goldberg, Cardiomyocyte expression of PPARgamma leads to cardiac dysfunction in mice, J. Clin. Invest. 117 (10) (2007) 2791–2801, https://doi.org/10.1172/JCI30335.

[29] N.H. Son, S. Yu, J. Tuinei, K. Arai, H. Hamai, S. Homma, G.I. Shulman, E.D. Abel, I. J. Goldberg, PPARgamma-induced cardiolipotoxicity in mice is ameliorated by PPARalpha deficiency despite increases in fatty acid oxidation, J. Clin. Invest. 120 (10) (2010) 3443–3454, https://doi.org/10.1172/JCI40905.

[30] P. Dobrzyn, H. Sampath, A. Dobrzyn, M. Miyazaki, J.M. Ntambi, Loss of stearoyl-CoA desaturase 1 inhibits fatty acid oxidation and increases glucose utilization in the heart, Am. J. Physiol. Endocrinol. Metab. 294 (2) (2008) E357–E364, https://doi.org/10.1152/ajpendo.00471.2007.

[31] Y. Zhou, L. Zhong, S. Yu, W. Shen, C. Cai, H. Yu, Inhibition of stearoyl-coenzyme A desaturase 1 ameliorates hepatic steatosis by inducing AMPK-mediated lipophagy, Aging (Albany NY) 12 (8) (2020) 7350–7362, https://doi.org/10.18632/aging.103082.

[32] A. Dziewulska, A.M. Dobosz, A. Dobrzyn, A. Smolinska, K. Kolczynska, J. M. Ntambi, P. Dobrzyn, SCD1 regulates the AMPK/SIRT1 pathway and histone acetylation through changes in adenine nucleotide metabolism in skeletal muscle, J. Cell. Physiol. 235 (2) (2020) 1129–1140, https://doi.org/10.1002/jcp.29026.

[33] Q.A. Wang, F. Zhang, L. Jiang, R. Ye, Y. An, M. Shao, C. Tao, R.K. Gupta, P. E. Scherer, Peroxisome proliferator-activated receptor gamma and its role in adipocyte homeostasis and thiazolidinedione-mediated insulin sensitization, Mol. Cell Biol. 38 (10) (2018), https://doi.org/10.1128/MCB.00677-17.

[34] T. Satoh, M. Toyoda, H. Hoshino, T. Monden, M. Yamada, H. Shimizu, K. Miyamoto, M. Mori, Activation of peroxisome proliferator-activated receptor-gamma stimulates the growth arrest and DNA-damage inducible 153 gene in non-small cell lung carcinoma cells, Oncogene 21 (14) (2002) 2171–2180, https://doi.org/10.1038/sj.onc.1205279.

[35] L. Fang, M. Zhang, Y. Li, Y. Liu, Q. Cui, N. Wang, PPARgene: a database of experimentally verified and computationally predicted PPAR target genes, PPAR Res. 2016 (2016) 6042162, https://doi.org/10.1155/2016/6042162.

[36] M.J. Khandekar, A.S. Banks, D. Laznik-Bogoslavski, J.P. White, J.H. Choi, L. Kazak, J.C. Lo, P. Cohen, K.K. Wong, T.M. Kamenecka, P.R. Griffin, B.M. Spiegelman, Noncanonical agonist PPARgamma ligands modulate the response to DNA damage and sensitize cancer cells to cytotoxic chemotherapy, Proc. Natl. Acad. Sci. U. S. A. 115 (3) (2018) 561–566, https://doi.org/10.1073/pnas.1717776115.

[37] J.K. Hennigs, A. Cao, C.G. Li, M. Shi, J. Mienert, K. Miyagawa, J. Korbelin, D. P. Marciano, P.I. Chen, M. Roughley, M.V. Elliott, R.L. Harper, M.A. Bill, J. Chappell, J.R. Moonen, I. Diebold, L. Wang, M.P. Snyder, M. Rabinovitch, PPARgamma-p53-Mediated vasculoregenerative program to reverse pulmonary hypertension, Circ. Res. 128 (3) (2021) 401–418, https://doi.org/10.1161/CIRCRESAHA.119.316339.

[38] C.G. Li, C. Mahon, N.M. Sweeney, E. Verschueren, V. Kantamani, D. Li, J. K. Hennigs, D.P. Marciano, I. Diebold, O. Abu-Halawa, M. Elliott, S. Sa, F. Guo, L. Wang, A. Cao, C. Guignabert, J. Sollier, N.P. Nickel, M. Kaschwich, K. A. Cimprich, M. Rabinovitch, PPARgamma interaction with UBR5/ATMIN promotes DNA repair to maintain endothelial homeostasis, Cell Rep. 26 (5) (2019) 1333–1343 e7, https://doi.org/10.1016/j.celrep.2019.01.013.

[39] A. Rasool, T. Mahmoud, P. O'Tierney-Ginn, Lipid aldehydes 4-hydroxynonenal and 4-hydroxyhexenal exposure differentially impact lipogenic pathways in human placenta, Biology 12 (4) (2023), https://doi.org/10.3390/biology12040527.

[40] K.A. Burns, J.P. Vanden Heuvel, Modulation of PPAR activity via phosphorylation, Biochim. Biophys. Acta 1771 (8) (2007) 952–960, https://doi.org/10.1016/j.bbalip.2007.04.018.

[41] R. Ventura-Clapier, A. Garnier, V. Veksler, Transcriptional control of mitochondrial biogenesis: the central role of PGC-1alpha, Cardiovasc. Res. 79 (2) (2008) 208–217, https://doi.org/10.1093/cvr/cvn098.

[42] S.M. Yeligar, B.Y. Kang, K.M. Bijli, J.M. Kleinhenz, T.C. Murphy, G. Torres, A. San Martin, R.L. Sutliff, C.M. Hart, PPARgamma regulates mitochondrial structure and function and human pulmonary artery smooth muscle cell proliferation, Am. J. Respir. Cell Mol. Biol. 58 (5) (2018) 648–657, https://doi.org/10.1165/rcmb.2016-0293OC.

[43] F.X.R. Sutandy, I. Gossner, G. Tascher, C. Munch, A cytosolic surveillance mechanism activates the mitochondrial UPR, Nature 618 (7966) (2023) 849–854, https://doi.org/10.1038/s41586-023-06142-0.

[44] F. Ishikawa, T. Akimoto, H. Yamamoto, Y. Araki, T. Yoshie, K. Mori, H. Hayashi, K. Nose, M. Shibanuma, Gene expression profiling identifies a role for CHOP during inhibition of the mitochondrial respiratory chain, J. Biochem. 146 (1) (2009) 123–132, https://doi.org/10.1093/jb/mvp052.

[45] S. Sjostedt, G. Rooth, F. Caligara, The oxygen tension of the amniotic fluid, Am. J. Obstet. Gynecol. 76 (6) (1958) 1226–1230, https://doi.org/10.1016/s0002-9378(16)36937-x.